



A Single Valve Brass Instrument Model using Finite-Difference Time-Domain Methods

R. Harrison and J. Chick

University of Edinburgh, Acoustics and Audio Group, EH9 3JZ Edinburgh, UK
r.l.harrison-3@sms.ed.ac.uk

Performance of a valved brass instrument, as for all musical instruments, is inherently time varying. In addition to lip dynamics the player also has control over the length of the air column through the use of valves; to date, this time-varying feature of the instrument has seen relatively little work at either the experimental or theoretical level. Three situations can be considered when investigating valve effects on a brass instrument: static, fully depressed; static, partially depressed; and a time-varying transition between valve configurations. In a static setting, fully depressing a valve increases the total tube length, thus lowering the resonance frequencies of the instrument. In static, partially depressed configuration, the effect on the input impedance is nontrivial due to the existence of multiple paths and constrictions that increase the boundary layer effects. Finally, during transitions between configurations, transient effects on the wave propagation cannot be ignored.

This paper presents a finite-difference time-domain (FDTD) model of a brass instrument with a single working valve. FDTD methods allow for the flexible simulation of time varying systems and are therefore well suited to the synthesis of brass instrument sounds, as well as experimental validation. Experimental impedance measurements of a simplified brass instrument are made for the instrument under static conditions. These measurements are then compared to the simulation results to verify the model. Future work is then considered for the time varying valve configurations and how these could be investigated in the laboratory.

1 Introduction

The effect of a brass instrument valve can be considered as a diversion of the airflow through different paths in the instrument. In general, there are two possible paths: the default, where the air flows straight through the valve; and the bypass, where the valve diverts the air into a longer piece of tubing which then rejoins the bore at the exit of the default tube. In the latter case, the airflow passes through the valve twice.

Finite-Difference Time-Domain (FDTD) methods are well suited to the simulation of time-varying systems and have been shown to be well suited to the simulation of musical instruments[1]. Although more computationally expensive than other time-domain methods, such as digital waveguides, they do allow for accurate simulation of system dynamics and allow for flexible user control in musical applications. The model used is presented in Section 2 followed by the finite-difference schemes in Section 3. Valve junctions are discussed in Section 4. Preliminary experiments performed on a simplified valved instrument are described in Section 5 and then the experimental and simulation results are presented in Section 6. Further work is discussed alongside the concluding remarks in Section 7.

2 Tube Model

For static wall conditions and oscillatory flow, the air pressure, p , and velocity, v , in an acoustic tube can be described in one dimension using acoustic impedance, Z , and admittance, Y , so that[2]

$$\partial_x \hat{p} = -Z \hat{v} \quad (1)$$

$$\partial_x S \hat{v} = -Y S \hat{p} \quad (2)$$

where ∂_x corresponds to the first derivative along the axial length of the tube, S corresponds to the cross-sectional area of the air column and the $\hat{\cdot}$ operator is used to distinguish the frequency domain pressure and velocity functions, \hat{p} and \hat{v} , from the time domain pressure and velocity functions. The impedance and admittance include losses associated with viscothermal boundary layers and are defined as

$$Z = \frac{j\omega R_0}{c(1 - F(r_v))}, Y = \frac{j\omega(1 + (\gamma - 1)F(r_t))}{cR_0} \quad (3)$$

where

$$F(\phi) = \frac{2}{\phi} \frac{J_1(\phi\sqrt{-j})}{\sqrt{-j} J_0(\phi\sqrt{-j})} \quad (4)$$

where $j = \sqrt{-1}$, $R_0 = \frac{\rho c}{\pi a^2}$, a is the air column radius and

$$r_v = a \left(\frac{\rho \omega}{\eta} \right)^{\frac{1}{2}}, r_t = P_r r_v \quad (5)$$

represent the ratio of the air column radius to the viscous and thermal boundary layers respectively. Other symbols denote thermodynamic constants and are defined in the Table 1.

Benade[2], Caussé *et al*[3] and Keefe[4] have all derived approximations to the impedance and admittance for different limits of r_v and r_t . Keefe gave approximations for cases where $r_v > 1$, the large r approximation, and $r_v < 1$, the small r approximation, that allowed for a smooth transition region around unity. By defining $Z = j\omega L + R$ and $Y = j\omega C + G$, the large r approximation is given by

$$R = R_0 \left(\frac{\omega}{c} \sqrt{2} \right) r_v^{-1} \left[1 + \frac{3r_v^{-1}}{\sqrt{2}} + \frac{15r_v^{-2}}{8} \right] \quad (6)$$

$$\omega L = R_0 \left(\frac{\omega}{c} \right) \left(1 + \sqrt{2} r_v^{-1} - \frac{r_v^{-3}}{\sqrt{2}} \right) \quad (7)$$

$$G = \frac{\sqrt{2}\omega}{cR_0} (\gamma - 1) r_t^{-1} \left(1 - \frac{r_t^{-1}}{\sqrt{2}} - \frac{r_t^{-2}}{8} \right) \quad (8)$$

$$\omega C = \frac{\omega}{cR_0} \left(1 + (\gamma - 1) \sqrt{2} r_t^{-1} \left(1 + \frac{r_t^{-2}}{8} \right) \right) \quad (9)$$

and the small r approximation¹ is given by

$$R = \frac{8\eta}{\pi a^4} \quad (10)$$

$$\omega L = \frac{4\rho\omega}{3\pi a^2} \quad (11)$$

$$G = \frac{\pi a^4 \omega^2}{8\rho c^2} (\gamma - 1) \rho \frac{P_r^2}{\eta} \left(1 - \frac{13r_t^4}{384} \right) \quad (12)$$

$$\omega C = \frac{\pi a^2 \omega \gamma}{\rho c^2} \quad (13)$$

¹note that in the original paper[4] there appears to be a typographical error in the definition of G and ωL which has been corrected here

Using these approximations, the characteristic impedance of a cylindrical tube can be calculated as

$$Z_c = (Z/Y)^{0.5} \quad (14)$$

Constant	Value
Air Density, ρ [kgm ⁻³]	1.1769 (1 - 0.00335 ΔT)
Speed of Sound, c [ms ⁻¹]	347.23 (1 + 0.00166 ΔT)
Viscosity, η [kgs ⁻¹ m ⁻¹]	(1.846 $\times 10^{-5}$) (1 + 0.0025 ΔT)
Prandtl Number, P_r	0.841 (1 - 0.0002 ΔT)
Ratio of Specific heats, γ	1.41017 (1 - 0.00002 ΔT)

Table 1: List of thermodynamic constants as reproduced from Benade[2] and reprinted by Keefe[4], where ΔT is the temperature variation from 26.85°C

Considering paths that lie entirely within either the default or bypass tube, the surface area of the acoustic wave has a larger diameter than the boundary layers associated with viscothermal losses within the frequency range of interest in brass instrument playing. This means that the large r approximation derived by Keefe[4] can be used to simulate these losses, as has been done in previous work on instrument simulation[5]. In partially opened valve configurations, the large r approximation is not always correct as one can imagine a situation where the valve has a very small opening into either the default or bypass tube. In this case the small r approximation must be used. To the authors' knowledge no previous work on trumpet valves has considered this change in behaviour for small valve constrictions.

3 Finite-Difference Time-Domain Formulation

A discrete time-domain formulation of the system can be obtained from the frequency domain through the transformation $(j\omega)^m \rightarrow \partial_m$ in Eqs. (1) and (2) when Z and Y are evaluated using Eqs. (6) to (9) for the large r approximation and Eqs. (10) to (13) for the small r approximation.

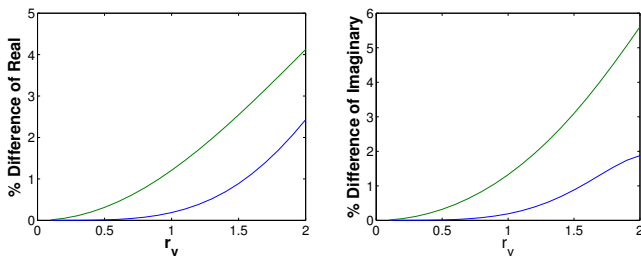


Figure 1: Percentage difference of the characteristic impedance, Z_c , using the small r approximation using G defined in Eq. (12) (blue) and $G = 0$ (green) from the exact solution. Top is real part, bottom is imaginary part

For preliminary investigation G in Eq. (12) is assumed, for convenience, to be zero to allow the order of the differential equations be the same for small and large r approximations. Figure 1 shows the percentage difference of the characteristic

impedance, Eq. (14), using the small r approximation with G set by Eq.(12) and set to zero from the exact solution. Both settings yield a difference of less than 6% over the accepted range of the approximation. The small r approximation becomes

$$\partial_x p = -\left(\frac{4\rho}{3S} \partial_t v + \frac{8\eta\pi}{S^2} v\right) \quad (15)$$

$$\partial_x S v = -\frac{S\gamma}{\rho c^2} \partial_t p \quad (16)$$

Note that Eqs. (15) and (16) do not reduce to Webster's equation.

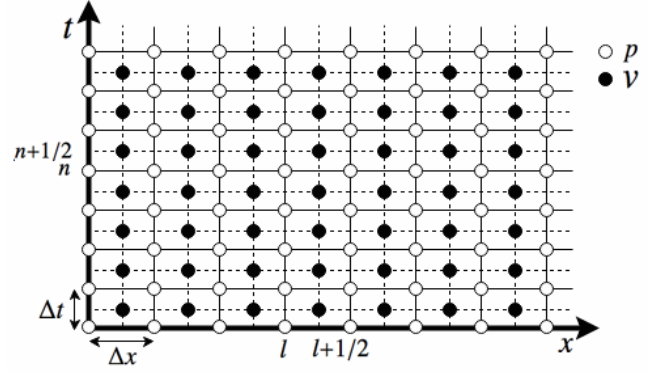


Figure 2: Discretisation of pressure and velocity fields.

Open circles are pressure nodes and filled circles are velocity nodes. Solid lines define integer time/space points and dashed lines define half-integer space/time points. l denotes spatial index spaced a distance Δx apart. n denotes time index spaced a time Δt apart.

To construct a finite-difference scheme for these equations, first the pressure and velocity fields are discretised and interleaved so that the pressure field values lie on integer space/time grid points and the velocity field lies on the half-integer grid points as shown in Figure 2. The partial derivative operators are then replaced with either forward or backwards finite difference operators depending on which is required for centring of the equations[5, 6]. For arbitrary variable i , the forwards and backwards difference operators are defined

$$\partial_i \rightarrow \delta_{i+} = \frac{e_{i+} - 1}{\Delta i}, \quad \partial_i \rightarrow \delta_{i-} = \frac{1 - e_{i-}}{\Delta i} \quad (17)$$

where e_{i+} and e_{i-} define shifting operators that translate a function either one step forwards or backwards respectively. Δi refers to the grid spacing for that variable. Similarly forwards and backwards averaging operators can be defined as

$$\mu_{i+} = \frac{e_{i+} - 1}{2}, \quad \mu_{i-} = \frac{1 - e_{i-}}{2} \quad (18)$$

for necessary centring requirements (for more information on FDTD operators see [1]).

The finite-difference scheme for the small r approximation is

$$\delta_{x+} p_l^n = -\left(\frac{4\rho}{3S_{l+1/2}} \delta_{t-} v_{l+1/2}^{n+1/2} + \frac{8\eta\pi}{S_{l+1/2}^2} \mu_{t-} v_{l+1/2}^{n+1/2}\right) \quad (19)$$

$$\delta_{x-} (S_{l+1/2} v_{l+1/2}^{n+1/2}) = -\frac{\bar{S}\gamma}{\rho c^2} \delta_{t+} p_l^n \quad (20)$$

The large r approximation can be simplified to a lower order;

with Z truncated to $O(r_v^{-2})$ and Y truncated to $O(r_t^{-1})$ to create positive, real functions[5]

$$Z = \rho\omega \left(j + \frac{2j^{1/2}}{r_v} + \frac{3}{r_v^2} \right) \quad (21)$$

$$Y = \frac{\omega}{\rho c^2} \left(j + \frac{2(\gamma-1)j^{1/2}}{r_t} \right) \quad (22)$$

This leads to the finite-difference scheme

$$\delta_{x+} p_l^n = - \left(\rho \delta_{t-} v_{l+1/2}^{n+1/2} + f_{l+1/2} \mu_{t-} v_{l+1/2}^{n+1/2} + g_{l+1/2} \delta_{t^{1/2}} \mu_{t-} v_{l+1/2}^{n+1/2} \right) \quad (23)$$

$$\delta_{x-} \left(S_{l+1/2} v_{l+1/2}^{n+1/2} \right) = - \left(\frac{\bar{S}_l}{\rho c^2} \delta_{t+} p_l^n + q_l \delta_{t^{1/2}} \mu_{t+} p_l^n \right) \quad (24)$$

where subscript l is the spatial index and superscript n refers to time index. \bar{S}_l is defined as $\bar{S}_l = \mu_{x-} S_{l+1/2}$ and

$$f_{l+1/2} = \frac{3\eta\pi}{S_{l+1/2}}, \quad g_{l+1/2} = 2 \sqrt{\frac{\rho\eta\pi}{S_{l+1/2}}} \quad (25)$$

$$q_l = \frac{2(\gamma-1)}{P_r c^2} \sqrt{\frac{\eta\pi \bar{S}_l}{\rho^3}}$$

For numerical stability, the spacing of the grid is set by the Courant Friedrichs Lewy[7] condition

$$\frac{c\Delta t}{\Delta x} \leq 1 \quad (26)$$

where Δt is the time step (inverse sample rate) and Δx is the length step. The fractional derivatives in Eqs. (23) and (24) are approximated in the same way as Bilbao and Chick[5]. This involves taking a Taylor expansion of the numerator and denominator of the Tustin transformation[8, 9] and then generating a continued fraction expansion using the method described by Sakurai et al[10]. The continued fraction expansion is then truncated and rearranged to create a polynomial fraction of order M which is normalised so that the zeroth order denominator coefficient is unity.

$$\delta_{t^{1/2}} \rightarrow \sqrt{\frac{2}{\Delta t}} (1 - e_{t-})^{0.5} (1 + e_{t-})^{-0.5} \rightarrow A^{-1} B \quad (27)$$

$$B = \sum_{r=0}^M b_r e_{t-}^r, \quad A = \sum_{r=0}^M a_r e_{t-}^r, \quad a_0 = 1 \quad (28)$$

4 Valve Junctions

Consider the valve schematic in Figure 3.

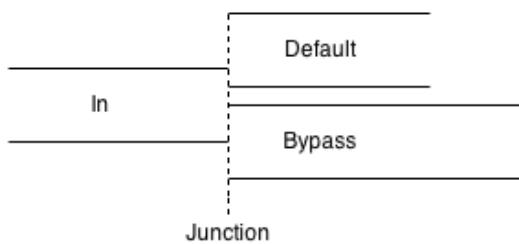


Figure 3: Valve schematic. Input tube feeds into the default and bypass sections

At the valve junction it is assumed that the pressure is the

same at the boundary of all tubes and the volume velocities sum to zeros[6].

$$p_J^n = p_{in}^n = p_d^n = p_{by}^n \quad (29)$$

$$\mu_{x+} \left(S_{in} v_{in}^{n+1/2} \right) = \mu_{x-} \left(S_d v_{d1/2}^{n+1/2} \right) + \mu_{x-} \left(S_{by} v_{by1/2}^{n+1/2} \right) \quad (30)$$

Where subscripts in , d and by refer to the input, default and bypass tubes and J refers to the junction point. At the junction the area of the default and bypass tubes are ratios q_d and q_{by} of the input tube

$$S_d = q_d S_{in}, \quad S_{by} = q_{by} S_{in} \quad (31)$$

$$q_d + q_{by} \leq 1 \quad (32)$$

where Eq.(32) can be less than unity because the geometry of the tubing means that the input tube does not completely overlap the default and bypass tubes. The pressure update at the junction can be calculated using either Eq.(24) or (20) depending on the individual tube radii and using the identity

$$\delta_{i-} = \frac{2}{\Delta i} (\mu_{i-} - e_{i-}) = \frac{2}{\Delta i} (1 - \mu_{i-}) \quad (33)$$

For an input tube that branches into the default and bypass tubes at the valve, the pressure at the junction is defined by

$$2 \left(S v_{in}^{n+1/2} - S v_{d1/2}^{n+1/2} - S v_{by1/2}^{n+1/2} \right) = \left[\alpha \delta_{t+} + \beta A^{-1} B \mu_{t+} \right] p_J^n \quad (34)$$

For all tubes large enough that the large r approximation holds

$$\alpha = \left(\Delta x_{in} + \Delta x_d q_d + \Delta x_{by} q_{by} \right) \frac{\bar{S}_J}{\rho c^2} \quad (35)$$

$$\beta = \left(\Delta x_{in} + \Delta x_d \sqrt{q_d} + \Delta x_{by} \sqrt{q_{by}} \right) \frac{2(\gamma-1)}{P_r c^2} \sqrt{\frac{\eta\pi \bar{S}_J}{\rho^3}} P_r \quad (36)$$

When the default and bypass tubes are defined using the small r approximation but the input uses the large r

$$\alpha = \left(\Delta x_{in} + \gamma \Delta x_d q_d + \gamma \Delta x_{by} q_{by} \right) \frac{\bar{S}_J}{\rho c^2} \quad (37)$$

$$\beta = \Delta x_{in} \frac{2(\gamma-1)}{P_r c^2} \sqrt{\frac{\eta\pi \bar{S}_J}{\rho^3}} \quad (38)$$

The definitions for α and β can be appropriately mixed if one of the default or bypass tubes uses the large r approximation and the other uses the smaller. Note that individual length spacings of each tube must be used due to effects related to discretising each tube section.

5 Experimental Procedure

To explore the effects of a valved transition, a simplified brass instrument was constructed consisting of a single (Perinet) valve from a standard Bb orchestral trumpet, coupled to lengths of cylindrical tubing of nominally similar diameter to that used in the valve section of the trumpet (11.6mm). A schematic of the experimental setup is shown in Figure 4. With the valve open the default tube length was 2492mm, and with the valve depressed, this was extended by 217mm (the length of the third valve tubing on a Bb trumpet using the first valve slide to remove effects related

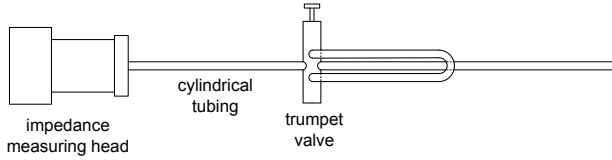


Figure 4: Schematic of the experimental setup used to measure the input impedance at different stages of a valve transition.

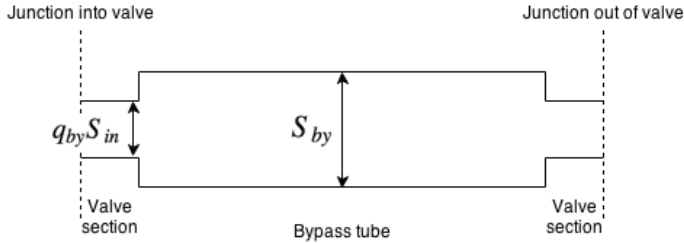


Figure 5: Schematic of bypass section used in simulations. The valve sections are assumed to be constrictions of the air flow therefore only two junctions are considered.

to the water key).

The acoustic impedance of the test instrument was measured using the BIAS capillary-based impedance measurement system [11, 12]. Measurements were taken with the valve fully ‘open’. The valve was then progressively depressed in 2mm increments using machined spacers to positively locate the valve at different stages of the transition from ‘open’ to ‘closed’. An impedance measurement was taken at each increment until the valve was fully depressed.

6 Simulation and Experimental Results

Impedance measurements of the experiment and those calculated using the finite-difference schemes presented in this paper are shown in Figure 6. Simulations were run at a sample rate of 44.1kHz for 1s and at a temperature of 23°C. The order of the large r viscothermal filter was 20. The values of q_d and q_{by} were calculated using the ratios of overlapping circles. The small r approximation was applied when the air column radius was less than 1mm. The radiation model of an unflanged circular pipe presented by Bilbao and Chick[5] was used as the output boundary condition and an impulse was used as the volume velocity, u , where $u = \mu_{x-} (S_{1/2} v_{1/2}^{n+1/2}) = 1$ for $t = 0$ and 0 otherwise, for the calculation of the pressure at the input using a lossless finite-difference scheme in Eq.(39)

$$\frac{\bar{S}_0}{\rho c^2} \delta_{t+} p_0^n = -\frac{2}{\Delta x} (S_{1/2} v_{1/2}^{n+1/2} - u^{n+1/2}) \quad (39)$$

For the bypass path, the valve sections were considered to be a constriction in the bypass tube and therefore junctions were only only considered where the tube connected to the input and output sections of tubing as shown in Figure 5. In the valve sections of the air column it is assumed that the cross sectional area is the same as the opening of that valve section and that the air column does not expand to the full

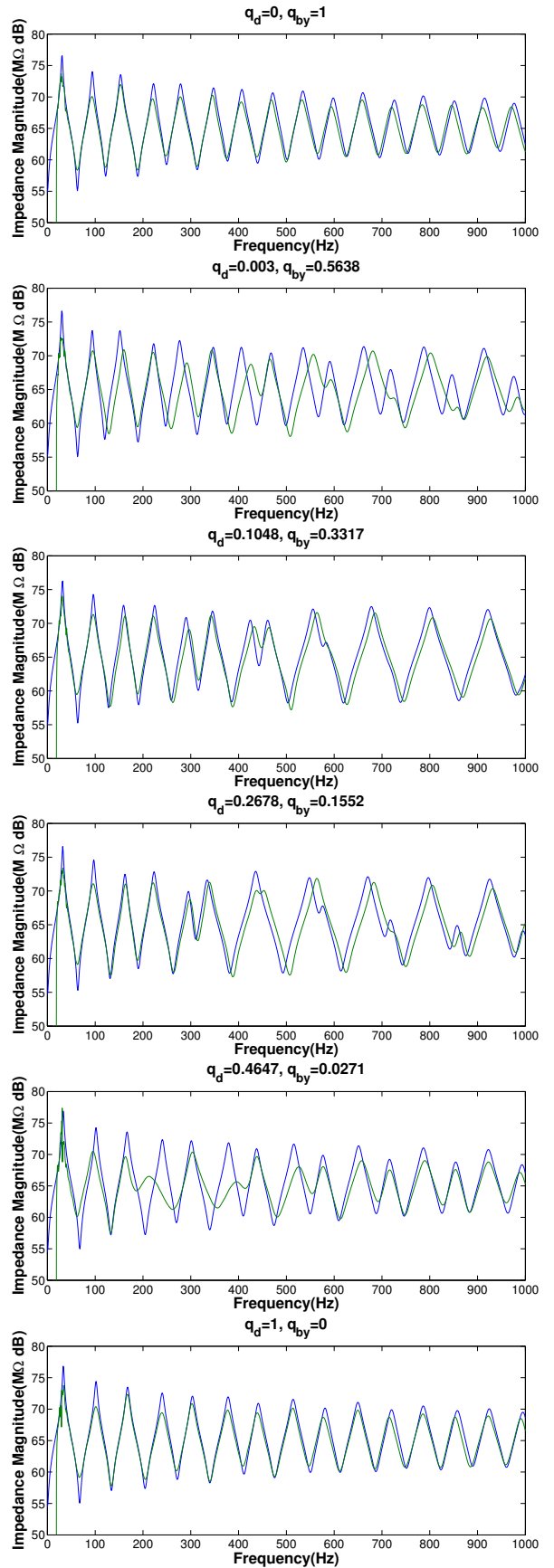


Figure 6: Measured (green) and simulated (blue) impedances for different valve openings. Top to bottom corresponds to gradually opening the valve. $q_d = 0.003$ and $q_{by} = 0.0271$ are instances when the small r approximation for viscothermal losses is used.

tube area until it reaches the longer length of tubing.

The experimental results show that when the valve is in a partially open configuration new peaks begin to emerge in the impedance measurements. The simulation results match experiment well for the fully closed and open valve configurations and follow behaviour for partial valve configurations, although less well matched for the case when the valve ratios are $q_d = 0.003$ and $q_{by} = 0.0271$. This could be down to experimental error in determining the opening of the valve section or the change in shape of the air column at the valve junction. Another source of difference between the simulation and experiment could be due to limitations in the small r scheme chosen and could be improved through the use of non zero G in equation 12. For $q_d = 0.1048$ and $q_d = 0.2678$, cases when the large r approximation is used in all tubes, the simulated impedances match well with those found in experiment especially at low frequencies. At higher frequencies there are some peaks predicted in the simulation that are not found in the experimental results; this could also be due to errors in calculating the opening of the valve junctions. Another source of error in the simulation could come from neglecting any effect of tight bends in the bypass path.

7 Conclusions and Further Work

This work intended to increase the literature on the study of brass instrument valves in partial configurations. The simplified instrument is a good starting point for this investigation, opposed to using real instruments, as it removes effects related to the complex geometries of instrument bores. The propagation and radiation of sound from open cylindrical pipes is also well understood which allows for focus on what happens at the valve boundaries. The FDTD scheme for the large r viscothermal approximation has already been shown to be appropriate for simulation of wave propagation in brass instruments[5, 6] and has proved to be successful for branching tubes in this example. The scheme for the small r approximation still requires further experimental and theoretical investigation.

One area that requires further investigation is how the air column changes shape when it reaches the valve junction. In this work it is assumed that the air column remains at constant area when it travels through the valve but this may not be the case. If the air column rapidly expands it could introduce turbulence into the system which may not be fully modelled in one dimension. Further experiments using custom made valves would allow for more control over the geometry of the default and bypass paths the airflow can travel through and would also remove the possibility of air leaks around the junction. These valves could potentially be made using 3-D printing technology which allows for flexible design and is becoming a more commercially viable method of construction. Custom built valves would allow for investigations into time-varying valve configurations as it would allow for positioning of microphones inside the valve. A full theoretical investigation into time varying valve configurations is also worth investigating as energy and stability analysis of FDTD scheme changes when tube walls vary with time.

8 Acknowledgement

Thanks go to Dr Stefan Bilbao and Dr Michael Newton for their useful discussions on this piece of research. This work was supported by the European Research Council, under grant number StG-2011-279068-NESS.

References

- [1] S. Bilbao. *Numerical Sound Synthesis: Finite Difference Schemes and Simulation in Musical Acoustics*. Wiley, 2009.
- [2] A. H. Benade. On the propagation of sound waves in a cylindrical conduit. *J. Acoust. Soc. Am.*, 44(2), 1968.
- [3] R. Caussé, J. Kergomard, and X. Lurton. Input impedance of brass musical instruments - comparison between experiment and numerical models. *J. Acoust. Soc. Am.*, 75(1), 1984.
- [4] D. H. Keefe. Acoustical wave propagation in cylindrical ducts: Transmission line parameter approximations for isothermal and nonisothermal boundary conditions. *J. Acoust. Soc. Am.*, 75(1), 1984.
- [5] S. Bilbao and J. Chick. Finite difference time domain simulation for the brass instrument bore. *J. Acoust. Soc. Am.*, 134(5), 2013.
- [6] S. Bilbao. Modelling of brass instrument valves. In *Proc. of the 14th International Conference on Digital Audio Effects*, Paris, France, September 2011.
- [7] R. Courant, K. Friedrichs, and H. Lewy. On the partial differential equations of mathematical physics. *Math. Ann.*, 100, 1928.
- [8] B. Vinagre, I. Podlubny, A. Hernandez, and V. Feliu. Some approximations of fractional order operators used in control theory and applications. *Fractional Calculus and Applied Analysis*, 3, 2000.
- [9] Y. Chen and K. Moore. Discretization schemes for fractional-order differentiators and integrators. *IEEE Trans. Circuits Syst.*, 49(3), 2002.
- [10] T. Sakurai, T. Torii, and H. Sugiura. An iterative method for algebraic equation by padé approximation. *Computing*, 46, 1990.
- [11] G. Widholm, H. Pichler, and T. Ossmann. Bias: A computer-aided test system for brass wind instruments. *Audio Engineering Society Paper*, 1989.
- [12] G. Widholm. Brass wind instrument quality measured and evaluated by a new computer system. In *Proceedings of the 15th International Congress on Acoustics*, Trondheim, Norway, 1995.